Experimental Validation of Damping Model for a MEMS Bistable Electrostatic Energy Harvester

C H Nguyen[1], D S Nguyen[2] and E Halvorsen[1]

[1] Department of Micro- and Nanosystem Technology, Buskerud and Vestfold University College, Raveien 215, N-3184 Borre, Norway
[2] Department of Mechanical Engineering, University of California, Berkeley, USA

E-mail: Einar.Halvorsen@hbv.no

Abstract. This paper validates lumped models of an asymmetric bistable MEMS electrostatic energy harvester against measurements. A conventional model of constant damping coefficient turns out to be ineffective in predicting or reproducing the device response. This shortcoming is demonstrated by the effective damping coefficient obtained from fits to experimental results being far from constant under varying operating conditions. Therefore, two different nonlinear models of the damping force in polynomial form are introduced and investigated. We find that the experimental results are well reproduced over the entire range of measured acceleration amplitudes by modeling with a phenomenological nonlinear damping force which is a high-order polynomial in the velocity.

1. Introduction

In designing a vibration energy harvester, it is challenging to make the generator adapt to the wide range of ambient vibration spectra. Nonlinearity of suspensions has been exploited to extend the working frequency range of the energy harvesters. In this approach, advantage is taken of the nonlinear dynamical behavior resulting from softening spring, hardening spring or bistable character of the system stiffness [1–3]. For example, an electrostatic MEMS device with an asymmetric bistable suspension showed an experimental bandwidth up to 715 Hz centered at 700 Hz [4]. In [5], 2.5 times wider bandwidth was achieved in a bistable electromagnetic generator than in a monostable one. It can often be difficult to obtain close agreement with experimental responses when modeling these bistable devices.

Damping is important to the bandwidth because it strongly affects the jump frequencies in frequency sweeps [6]. Therefore, understanding the behaviour of damping against a variety of working conditions is needed for device performance prediction. In this work, a bistable electrostatic energy harvester is characterized and modelled. The common model with a linear damping force [7] misses essential physics in the device. Motivated by this, we introduce instead nonlinear damping-force models in the form of polynomials in velocity and displacement. We have investigated to which degree these different models of parasitic mechanical damping result in simulated responses that agree with experiments on an asymmetric, bistable MEMS electrostatic energy harvester.

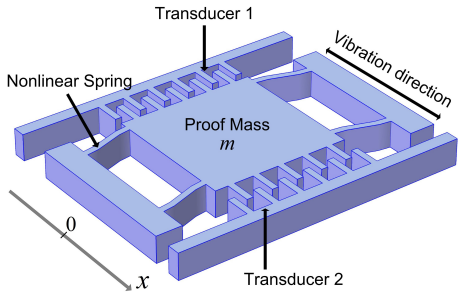

Figure 1. Schematic drawing of the bistable electrostatic energy harvester. The two capacitive transducers have different initial overlap areas.

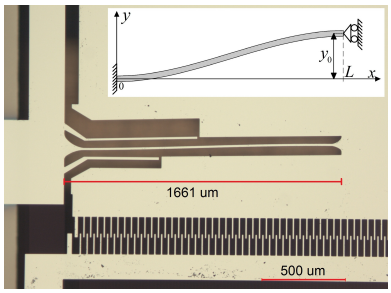

Figure 2. A corner of the device with a nonlinear spring and a part of transducer 2. Inset: drawing of the nonlinear spring $y_0 = 42\ \mu m$ and length $L = 1660\ \mu m$

2. Device Description and Characterisation

2.1. Bistable design of an electrostatic energy harvester

The harvester has a proof mass suspended by four springs as shown in figure 1. Taking advantage of the available space, two transducers, one on each side of the proof mass, are included in the generator. To obtain the bistable properties, the springs are designed to have a curved shape as shown in figure 2. The S-shaped springs have an initial displacement y_0 at the guided ends. The spring force vs. displacement curve, obtained by fitting the modeling to measurements, is shown in figure 3. For small displacements, the springs behave linearly around the 1^{st} stable position at 0. For further displacement in the positive direction, the spring is stiffer (or hardening) which is mainly due to tension. In the reverse direction, the springs are partly in compression resulting in a stiffness reduction or softening effect over part of the displacement range when some of the elastic energy is released. Decreasing the displacement from zero, the stiffness continues to decrease and reaches the instability point at the displacement of -30 μm and then the stable point at the displacement of -60 μm.

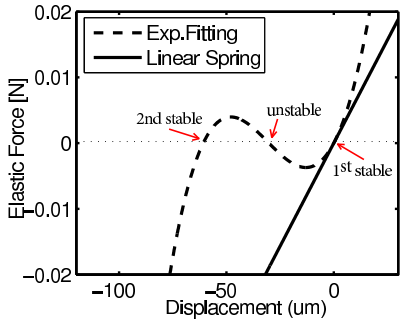

Figure 3. Nonlinear spring characteristic obtained from parameter fit. Linear spring is plotted for comparison

2.2. Characterisation method and results

For characterisation purposes, an external DC voltage is used for biasing of the device, a chirp excitation is taken as the input vibration source while the outputs of the generator are directly connected to resistive loads R_{L1}, R_{L2} at transducer 1 and transducer 2 respectively. The device is first characterized at several low acceleration amplitudes around 0.01 g to yield linear responses. Then, parameters such as the linear stiffness k_1, damping coefficient b, parasitic capacitance C_p and load capacitance C_L are determined from output voltage information, i.e. the resonant

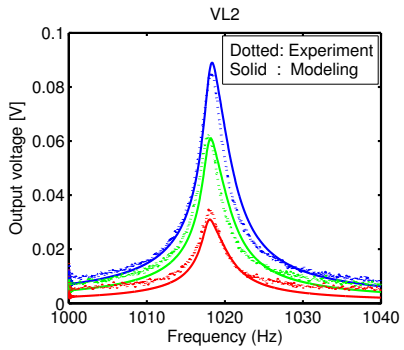

Figure 4. Output voltage at transducer 2 for acceleration amplitude of 0.01 g (linear regime) and bias voltage of 30 V, 20 V and 10 V (top to bottom)

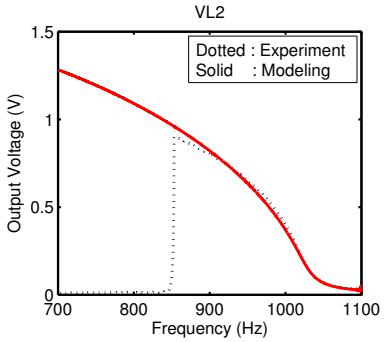

Figure 5. Output voltage at transducer 2 for acceleration amplitude of 0.28 g (nonlinear regime) and bias voltage of 20V.

frequency $f_0 = \frac{\omega_0}{2\pi} = \frac{1}{2\pi}\sqrt{\frac{k_1}{m}}$ and the quality factor $Q = \frac{f_0}{\Delta f} = \frac{m\omega_0}{b}$, where Δf is the bandwidth of the response. Next, in a range of higher acceleration amplitudes from 0.1 g to 0.3 g causing strong nonlinear effects, the higher-order stiffness parameters are obtained by fitting the output response from the device model with results from measurement. In this procedure, the previously established linear parameters are unchanged. The mass m and the dominant capacitor C_0 are calculated using the layout dimensions.

The parameters of the device are shown in Table 1. The linear behaviour of the generator is presented in figure 4 while the nonlinear one is shown in figure 5. As can be seen in the linear regime, the modeling results and experimental data are close with a small deviation far from the resonant frequency. The small deviation is due to noise in the measurement system. However, in the nonlinear regime, the amplitude of the voltage curve can only be fitted over a limited frequency range. The jump-down frequency is far from the observed value in the experiment. The same phenomenon was also observed for nonlinear piezoelectric energy harvester in [6].

The reason for this mismatch is that the linear damping is retained in our model for the nonlinear regime while in reality the situation is more complex. Experimentally this explanation is supported by the observation that the coefficient of the linear damping model needs to be adapted to the operation condition, i.e. acceleration amplitude and bias voltage, in order to reproduce the experiment results. This will be discussed in the next section.

3. Nonlinear Damping and Modeling

Figure 6 shows the effective linear damping value fitted to reproduce the experimental results for different conditions of the acceleration amplitude and the bias voltage. The effective linear damping is approximately linearly increasing when increasing the acceleration amplitude from 0 to 0.16 g and relatively constant beyond 0.16 g. We note that the effective damping curve depends on bias voltage, and that in particular the 30-V curve distinguishes itself from the 10-V and 20-V curves. We interpret this voltage dependence as a signature of inaccuracies in the representation of electrical damping which have little effect at 10-V and 20-V bias. We therefore conduct the remaining analysis at 20-V bias.

To describe the damping force that can give rise to effective damping coefficients as shown in figure 6, we introduce two models of the nonlinear damping force. One is a high-order polynomial in velocity and one is a third order form which also has displacement dependence:

Table 1. Bistable Electrostatic Energy Harvester Parameters

Notation	Description	Value	Unit
b	Linear damping coefficient	2.7x10^{-4}	Ns/m
m	Mass	15.18	mg
k_1	Linear stiffness	622	N/m
$k_{i=2:7}$	Nonlinear stiffness	2.96x10^{7} , 2.8x10^{11} , -4x10^{14} 1.06x10^{19}, 1.36x10^{23}, 4.2x10^{26}	Nm^{-i}
C_0^1, C_0^2	Transducer dominant capacitance	7.07, 1.75	pF
C_p^1, C_p^2	Transducer parasitic capacitance	14.5, 12.5	pF
C_L^1, C_L^2	Parasitic load capacitance	23, 8	pF
R_{L1}, R_{L2}	Load resistance	20.5, 20.5	MΩ

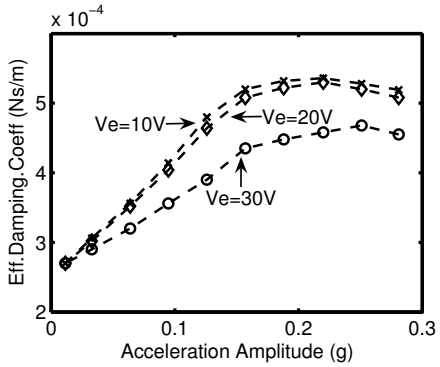

Figure 6. Effective damping coefficient extracted from measurements

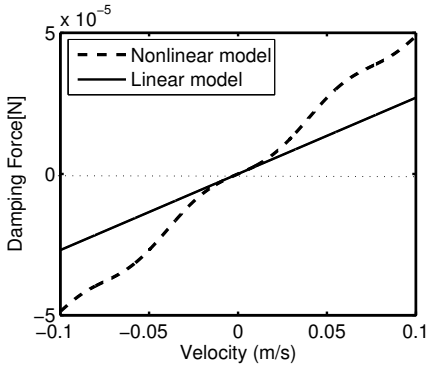

Figure 7. Nonlinear damping force obtained from parameter fit, compared to linear damper.

$$F_{nl\_damp}\left(\dot{x}\right) = b\dot{x} + \sum_{n=1}^{N} b_{2n+1}\left(\dot{x}\right)^{2n+1} \tag{1}$$

$$F_{nl\_damp}\left(x, \dot{x}\right) = b\dot{x} + b_{30}\left(\dot{x}\right)^{3} + b_{32}x^{2}\dot{x} \tag{2}$$

where $b_3 = 0.234\text{N(s/m)}^3$, $b_5 = -69.26\text{N(s/m)}^5$, $b_7 = 8.73 \times 10^3\text{N(s/m)}^7$, $b_9 = -4.98 \times 10^5\text{N(s/m)}^9$, $b_{11} = 1.06 \times 10^7\text{N(s/m)}^{11}$ and $b_{30} = 0.274\text{N(s/m)}^3$, and $b_{32} = -1.24 \times 10^7\text{Ns/m}^3$.

The form in (2) has been adopted from the analytic work on modeling of the nonlinear damping in a micromechanical oscillator in [8]. The high-order polynomial for the purely velocity-dependent nonlinear damping in (1) is mathematically motivated by the need capture a wide range of conceivable function forms. The damping force resulting from a fit to (1) is presented in figure 7 and is very different from the simple linear model $F = b\dot{x}$. The slope change in the force-velocity relation is made possible by using a 11^{th} order of polynomial. This form is able to reproduce the experimental results over a wide range of acceleration amplitudes as shown by the agreement with the experimental results in figure 8. The form (2) gives significantly worse fits as seen from the mismatch in the responses already at moderate acceleration amplitudes, i.e. above 0.19 g, in figure 9.

It is not clear what is the mechanism behind the nonlinear damping. However, this device has a low linear damping, i.e. $Q \approx 350$, due to the large gap of 500 μm between the mass and the substrate, and due to the even larger distance to the lid. Thus, gas flow in the finger

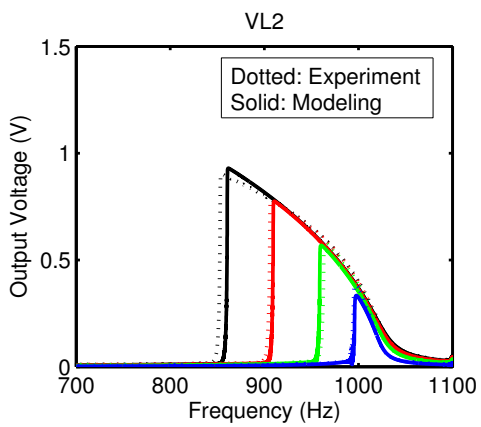

Figure 8. Output of transducer 2 with 11^{th} order polynomial damping force for acceleration amplitudes of 0.28 g, 0.25 g, 0.19 g, 0.1 g (left to right), bias voltage of 20 V.

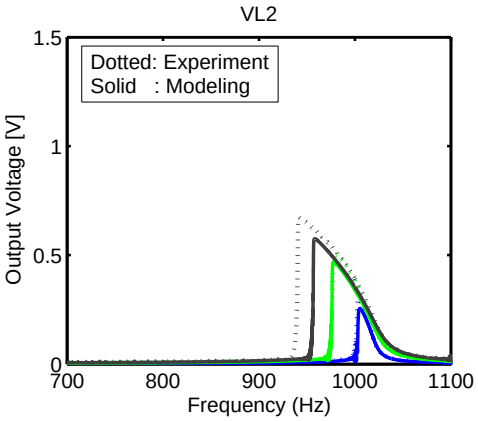

Figure 9. Output of transducer 2 with third-order velocity- and displacement-dependent damping force for acceleration amplitudes of 0.22 g, 0.19 g, 0.1 g (left to right), and bias voltage of 20 V.

structure is important for the damping, and could potentially include nonlinear effects at large displacements, which cause the gas volume within the finger structure to change significantly.

4. Conclusion

This paper investigated the behaviour of a bistable electrostatic energy harvester. It was demonstrated that the model of linear damping is not enough to reproduce the frequency response of this kind of device in the nonlinear regime. A systematic experiment was set up and revealed the dependency of the effective damping coefficient on excitation level and bias voltage. The bias-voltage dependence was used to indicate at which bias voltages one could expect inaccuracies in the electrical damping model to be insignificant for the mechanical damping estimates. Two different nonlinear damping models were fit to the experiment. A high-order expansion in velocity could successfully reproduce the experimental results. While this purely mechanical nonlinear damping can explain the device behavior as a function of acceleration amplitude, a physical explanation of the nonlinear damping is yet to be established and is a matter for further investigation.

Acknowledgments

This work was sponsored in part by the California Energy Commission under Grant no. 500-10-044, and in part by the Research Council of Norway under Grant. no. 229716/E20.

References

[1] A. Erturk, D. J. Inman, 2011 *J. Sound. Vib.* **330** pp 2339-2353
[2] S. C. Stanton, C. C. McGehee, B. P. Mann, 2010 *Physica D* **239** pp 640-653
[3] F. Cottone, L. Gammaitoni, H. Vocca, M. Ferrari, V. Ferrari 2012 *Smart Mater. Struc.* **21** 035021
[4] S. D. Nguyen, E. Halvorsen, I. Paprotny 2013 *Appl. Phys. Lett.* **102** 023904
[5] F. Cottone, P. Basset, H. Vocca, L. Gammaitoni, T. Bourouina 2014 *J.Intell. Mater Syst. Struct.* **25**
[6] G. Sebald, H. Kuwano, D. Guyomar, B. Ducharne 2011 *Smart. Mater. Struc.* **20** 10200
[7] S. D. Nguyen, E. Halvorsen 2009 *Proc. PowerMEMS* pp 411-414
[8] S. Zaitsev, O. Shtempluck, E. Buks, O. Gottlieb 2012 *Nonlinear. Dyn* **67** pp 859-883